Experimental evidence of surface conduction in AlSb–InAs tunneling diodes

K. Nomoto, K. Taira, T. Suzuki, and I. Hase
Research Center Sony Corporation, 174 Fujitsuka-cho, Hodogaya-ku, Yokohama 240, Japan

(Received 14 July 1998; accepted for publication 11 October 1998)

The peak-to-valley ratio of AlSb–InAs resonant tunneling diodes decreases as the diameter of the diode decreases due to the surface current. To clarify the origin of the surface current, we studied AlSb–InAs single-barrier diodes with various diameters and barrier thicknesses at various temperatures. We conclude from experimentally obtained results that bulk current is caused by tunneling through an AlSb barrier influenced by the band structure and surface current is caused by an electron emission from band-gap surface states at the AlSb barrier based on the Poole–Frenkel mechanism with ionization energy of 0.24 eV. © *1999 American Institute of Physics.* [S0021-8979(99)04302-9]

I. INTRODUCTION

Recently, submicrometer- or sub-0.1-μm-diam vertical multibarrier resonant tunneling structures and resonant tunneling diodes (RTDs) have attracted much attention, because they make it possible to study single-electron tunneling phenomena and Coulomb blockade effects,[1–5] to increase device density on a chip using RTD[6] and to reduce the capacitance that determines the oscillator frequency.[7,8] To date, most research has employed an AlGaAs–GaAs material system. Sub-0.1-μm-diam AlGaAs–GaAs RTDs are nonconductive, however, because the contact channel is pinched off by the surface depletion layer by the surface Fermi level pinning in the middle of the band gap of GaAs. On the other hand, the surface Fermi level of InAs is located just above or below the minimum of the conduction band and there is no surface depletion layer.[9,10] Therefore, InAs-based RTDs are expected to have no diameter limitation. Most research on InAs-based RTDs has been for high-frequency applications[7,8] and to understand the basic physics of tunneling phenomena as affected by the band structure.[11] Recently, we studied small diameter AlSb–InAs RTDs and reported that negative differential conductance was observed for AlSb–InAs double-barrier RTDs with a diameter down to 20 nm at room temperature.[12] We also reported in the letter that the peak-to-valley ratio (PVR) is reduced as the diameter of the RTD is reduced. For AlSb–InAs RTDs the contribution of the surface current to the valley current is the origin of the PVR degradation. The origin of the surface current is, however, unknown. PVR degradation was also observed for AlGaAs–GaAs RTDs.[2,13] This is due to the valley current density which increases as the diameter of the RTD decreases. There is, however, a debate about the origin of the increase in the valley current density.[2,13] In GaAs metal semiconductor field effect transistors, the current which flows between the gate and source through the surface state is observed.[14–17]

The purpose of this article is to clarify the mechanism of current conduction through AlSb–InAs RTDs and the origin of the PVR reduction in sub-μm-diam AlSb–InAs RTDs. The dependence of the current through the AlSb–InAs double-barrier RTDs and single-barrier diodes (SBDs) on the diameter, barrier thickness and temperature is studied. We conclude that the bulk current is caused by tunneling influenced by nonparabolic energy-momentum dispersion in the AlSb complex band structure in the band gap and the surface current, which is responsible for PVR degradation, is caused by Poole–Frenkel emission from the band-gap surface state of the AlSb barrier.

This article is organized as follows. In Sec. II, we will briefly review our previous results which show that the PVR of the AlSb–InAs RTDs decreases as the diode diameter decreases. Section III reports the dependence of conductance of AlSb SBDs with various AlSb barrier thicknesses on the diameter. In Sec. IV, we discuss the origin of the bulk current after investigating the conductance dependence on the AlSb barrier thickness. In Sec. V, the dependence of the $I(V)$ curve for AlSb–InAs SBD on temperature is studied to clarify the origin of the surface current.

II. PVR REDUCTION IN $I(V)$ CURVES FOR SUBMICROMETER-DIAMETER AlSb–InAs RTDs

In this section, we will review our experiments in which we observed that PVR is reduced as the diameter of AlSb–InAs double-barrier RTDs is reduced.

A. Sample description

The AlSb–InAs double-barrier layer structure was grown by molecular beam epitaxy (MBE) at 500 °C on a (001)-oriented 1×10^{18} cm^{-3} sulfur-doped n-type InAs substrate. The layer structure was as follows: (i) 600 nm n-InAs bottom contact layer ($n=1\times10^{18}$ cm^{-3}), (ii) 10 nm InAs spacer layer, (iii) 5 nm AlSb barrier, (iv) 6 nm InAs well, (v) 5 nm AlSb barrier, (vi) 10 nm InAs spacer layer, (vii) 100 nm n-InAs contact layer ($n=8\times10^{17}$ cm^{-3}), and (viii) 330 nm n^+-InAs top contact layer ($n=1\times10^{18}$ cm^{-3}). Silicon was used as the dopant. Layers (ii)–(vi) were undoped. The band diagram is shown in Fig. 1(a). AuGe/Au ohmic metalization dots with diameters of 2000–20 nm were defined on

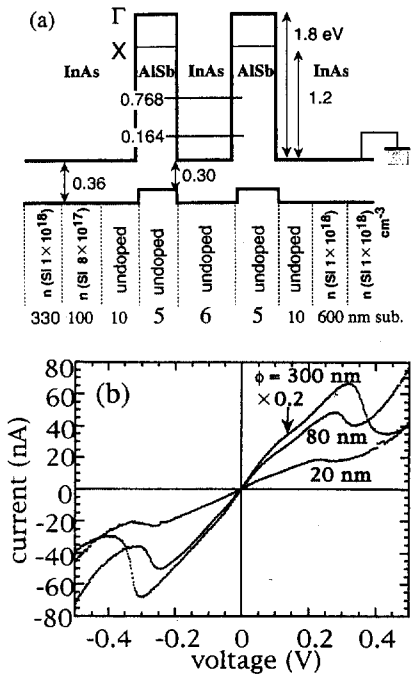

FIG. 1. (a) Schematic band diagram of the RTD investigated. The 2D subband energy is obtained from the calculation of the transmition probability for zero bias. (b) $I(V)$ curves at room temperature of three RTDs with diameters ϕ of 20, 80, and 300 nm.

n^+-InAs top contact using electron-beam lithography and the lift-off process. The details of the fabrication process are described in Ref. 12. Because InAs has a surface Fermi level around the conduction-band edge, we can obtain good ohmic contact without any heating process for all device. We confirmed that there is no surface leakage current through AlGaAs–GaAs RTDs fabricated using our process.

B. Diameter dependence of $I(V)$ characteristics

The $I(V)$ curves of AlSb–InAs RTDs with different diameters are shown in Fig. 1(b). The voltage is applied to the top contact with respect to the grounded substrate. The peaks at about ± 0.25 V are attributed to a resonant tunneling current through the lowest two-dimensional subband in the InAs quantum well. The bumps observed at ± 50 mV are interpreted as tunneling through an InAs Γ-point quasi-bound state confined by AlSb X-point barriers.[11]

As shown in Fig. 2, the PVR is reduced as the diameter of the RTD is reduced. In AlGaAs–GaAs RTDs this tendency has been already observed.[2,13] There is a debate about this decrease. In this debate, the weakened lateral-momentum-conservation rule derived from the Heisenberg uncertainty principle[2] and surface-related phenomena[13] are topics of discussion. To clarify the origin of PVR degradation in AlSb–InAs RTDs, we plot the diameter dependence of the peak current I_p, the valley current I_v and their difference $\Delta I = I_p - I_v$ at positive bias voltage at room temperature and at 4 K in Fig. 3. We observed the same characteristics for negative bias. We found no pinch-off for diodes with diameters down to 20 nm, as we expected. The current component ΔI is well fitted by the function $J_{RT}(\pi\phi^2/4)$, where the current density J_{RT} is given by 2.1×10^6 A/m^2, irrespective of temperature. Therefore ΔI is a resonant-tunneling-current component. On the other hand, for small diameter diodes, I_v is proportional to ϕ rather than ϕ^2 and thermally activated for all diameters. The valley current I_v is fitted by the sum of the bulk current and the surface current,

$$I_v = J_v(\pi\phi^2/4) + J_s(\pi\phi), \tag{1}$$

where $J_v = 1.2\times10^6$ A/m^2 and $J_s = 4.0\times10^{-1}$ A/m at room temperature and $J_v = 9.1\times10^4$ A/m^2 and $J_s = 5.7\times10^{-2}$ A/m at 4 K.

From these results, we conclude that (1) the resonant-tunneling-current density J_{RT} does not decrease as the diode diameter decreases, (2) the valley current contains a current component which is proportional to the diode circumference, and (3) the current component proportional to the diode circumference is thermally activated. We conclude from these

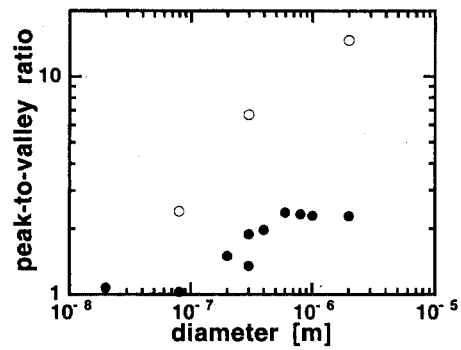

FIG. 2. Peak-to-valley ratio for AlSb–InAs RTDs as a function of diameter at room temperature (●) and 4 K (○).

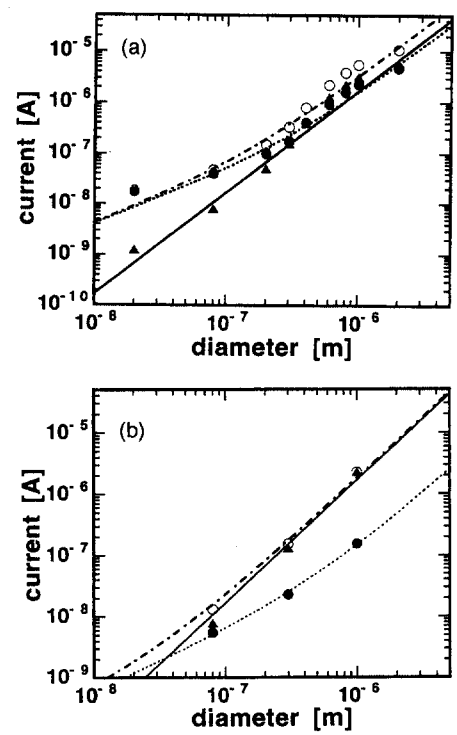

FIG. 3. Peak current (○) valley current (●) and resonant current (▲) at (a) room temperature and (b) 4 K as a function of RTD diameter. The best fitted ΔI, I_v curves and their sum $I_p = \Delta I + I_v$ are also shown.

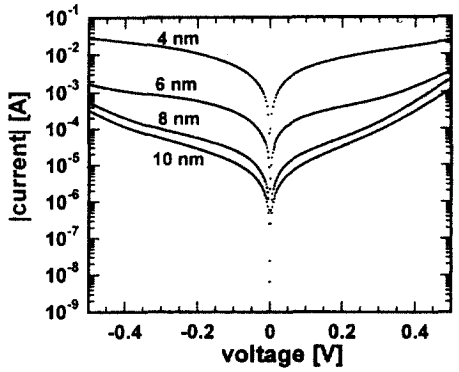

FIG. 4. $I(V)$ curves for AlSb–InAs SBD with a diameter of 100 μm and barrier thickness of 4, 6, 8, and 10 nm measured at room temperature.

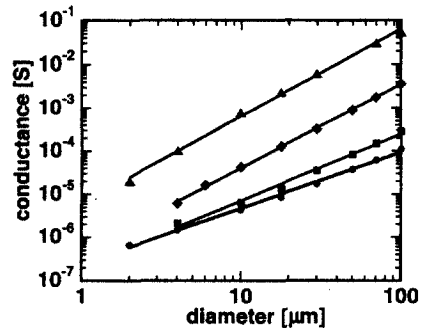

FIG. 5. Diameter dependence of zero-bias-voltage conductance of AlSb–InAs SBD with barrier thickness of 4 (▲), 6 (◆), 8 (■), and 10 nm (●) at room temperature. Each curve is fitted by the function $G=\alpha\phi^{\beta}$ with β=2.01 for 4 nm barrier, 1.94 for 6 nm barrier, 1.54 for 8 nm barrier, and 1.30 for 10 nm barrier AlSb–InAs SBDs.

results that the origin of the PVR degradation of AlSb–InAs RTDs is the thermally activated surface current, which is a component of the valley current. The side wall of the AlSb barrier layer is damaged by oxidation and the bombardment of ions during the fabrication process. This damage causes the band-gap surface defect levels. Conduction through these levels contributes to the thermally activated current.

In the following section, we will report the results of an experiment using AlSb–InAs SBD, which unambiguously shows the existence of a surface current through the AlSb barrier layer, and we will discuss the mechanism of conduction at the surface as well as in bulk.

III. DIAMETER DEPENDENCE OF THE CONDUCTANCE OF AlSb–InAs SBDs WITH VARIOUS AlSb BARRIER THICKNESSES

In this section, we will first describe the structure which we employed for the AlSb–InAs SBD, and then report the dependence of $I(V)$ characteristics on the AlSb barrier thickness and the diameter of the diode.

A. Sample description

The AlSb–InAs single-barrier layer structure was grown by MBE at 500 °C on a (001)-oriented 1×10^{18} cm^{-3} sulfur-doped n-type InAs substrate. The layer structure was as follows: (i) 600 nm n-InAs bottom contact layer ($n=1\times10^{18}$ cm^{-3}), (ii) 10 nm InAs spacer layer, (iii) AlSb barrier with thickness of d=4, 6, 8, or 10 nm, (iv) 10 nm InAs spacer layer, (v) 100 nm n-InAs contact layer ($n=8\times10^{17}$ cm^{-3}), and (vi) 330 nm n^+-InAs top contact layer ($n=1\times10^{18}$ cm^{-3}). Silicon was used as the dopant. Layers (ii)–(iv) were undoped. AuGe/Au ohmic contacts with diameters of 2–100 μm were defined on n^+-InAs top contact using photolithography. The ohmic metal was made using the same process as used for the AlSb–InAs RTD.

B. Results

Figure 4 shows a typical $I(V)$ curve of AlSb–InAs SBDs with AlSb barrier thickness of 4, 6, 8, and 10 nm and with the same diameter of 100 μm at room temperature. As we expected from the sample structure, the $I(V)$ curves are symmetric at the origin and the higher current flows through the thinner barrier AlSb SBDs.

In Fig. 5, we show the dependence of the conductance at zero bias voltage on the diameter of the AlSb SBDs with various barrier thicknesses. When the barrier thickness is less than ~8 nm, the conductance is proportional to ϕ^2 and therefore current flows in the bulk region. On the other hand, when the barrier thickness is larger than ~8 nm, the conductance is proportional to ϕ, which means that the surface current makes a major contribution to the total current.

As shown in Fig. 6, for the 4 nm barrier AlSb SBD, the conductance does not change with the temperature and is

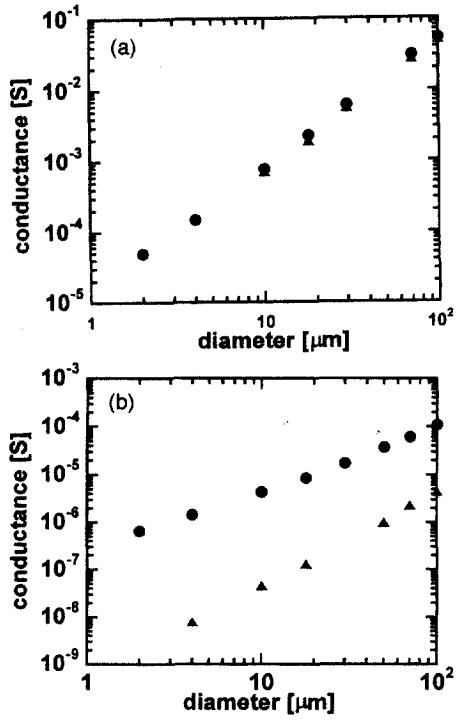

FIG. 6. Diameter dependence of zero-bias-voltage conductance of AlSb–InAs SBD (a) with barrier thickness of 4 nm at 77 K (▲) and room temperature (●) and (b) with barrier thickness of 10 nm at 77 K (▲) and room temperature (●).

proportional to ϕ^2. For the 10 nm barrier AlSb SBD, the conductance is proportional to ϕ^2 at 77 K. At room temperature, the conductance is, however, approximately proportional to ϕ and increases compared with the conductance at 77 K. These results suggest that a tunneling current makes a major contribution to the current through AlSb SBDs with a barrier thickness less than ~8 nm and that the thermally activated surface current dominates when the barrier thickness is larger than ~8 nm.

IV. THE ORIGIN OF THE BULK CURRENT

As discussed in the previous section, the diameter dependence of the AlSb SBD conductance suggests that the origin of the bulk current is a tunneling current through the AlSb barrier. To confirm this, we investigated the dependence of the conductance of the AlSb SBDs on the AlSb barrier thickness. The conductance G caused by tunneling at zero bias voltage and at zero temperature is given by the Landauer formula;

$$G=\frac{2e^2}{h}\sum_i T_i(E_{\mathrm{tot}}), \tag{2}$$

where E_{tot} is the energy of an tunneling electron, the index i denotes the available mode, excluding a spin, of a tunneling electron with the total energy E_{tot}, and $T_i(E_{\mathrm{tot}})$ is the tunneling probability of the ith mode electron with energy E_{tot}. For our samples, the index i is given by the momentum $\mathbf{k}_{\|}$ parallel to the interface of the barrier and therefore (2) becomes

$$G=S\frac{2e^2}{h}\int\frac{d^2\mathbf{k}_{\|}}{(2\pi)^2}T_{\mathbf{k}_{\|}}(E_{\mathrm{tot}}), \tag{3}$$

where S is the diode area. Hereafter, we use a separable model for the energy:

$$E_{\mathrm{tot}}=E_{\perp}+E_{\|}(\mathbf{k}_{\|}), \tag{4}$$

where $E_{\perp}$ and $E_{\|}$ are the components of the energy with respect to the degree of freedom in the direction perpendicular and parallel to the interface of the barrier, respectively. In order to compare the experimental results with theory in a simple way, we use the following approximation for the tunnel probability:

$$T_{\mathbf{k}_{\|}}(E_{\mathrm{tot}})=\exp\{-2\kappa[E_{\perp}]d\}, \tag{5}$$

$$E_{\perp}=E_{\mathrm{tot}}-E_{\|}(\mathbf{k}_{\|}). \tag{6}$$

The parameter $\kappa[E_{\perp}]$ is an imaginary wave vector normal to the AlSb–InAs interface in an AlSb.

We use the sp two-band tight-binding model to obtain the value of κ.[18–20] We define the on-site energy of the s orbit on the Sb and the p orbit on the Al by E_s and E_p, respectively, and define the transfer energy between the s orbit and the p orbit by t, the period of the Al–Sb plane by a (which is the half of the lattice constant of AlSb). and momentum by $k_{\perp}$. The imaginary wave vector κ is given by $\kappa=\mathrm{Im}\,k_{\perp}$. The band structure $E_{\perp}(k_{\perp})$ in the (001) direction is obtained by solving the following equation:

$$[E_{\perp}(k_{\perp})-E_s][E_{\perp}(k_{\perp})-E_p]=4t^2\sin^2(k_{\perp}a/2). \tag{7}$$

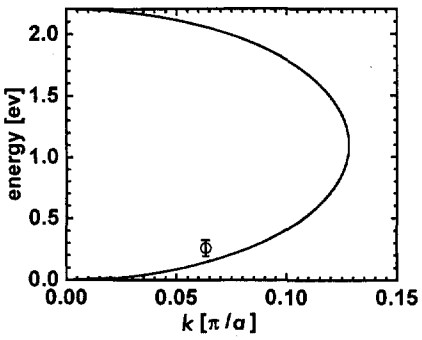

FIG. 7. Complex band structure in the band gap of AlSb. The solid curve is a calculated line based on the two band model. The circle (○) is experimental data which is obtained from the fitting in Fig. 8.

Here the transfer energy t and the electron effective mass have the following relation:

$$t^2=\frac{\hbar^2}{2m^*a^2}(E_s-E_p). \tag{8}$$

The energies E_s and E_p become the minimum energy of the conduction band and the maximum energy of the valence band, respectively. We use the value of $E_s-E_p=2.1$ eV which is equal to the band-gap energy of AlSb at Γ point and $a=0.614/2$ nm. The calculated band structure in the band gap for AlSb ΓX is shown in Fig. 7, where the maximum energy of the valence band is taken to be at the origin.

To estimate the momentum κ from the experimental results, we will simplify the expression (3). We assume that κ and therefore $T_{\mathbf{k}_{\|}}$ are constant in this energy range and $E_{\|}$ has a parabolic dispersion relation of $\mathbf{k}_{\|}$. Then the integration with respect to the momentum $\mathbf{k}_{\|}$ gives a simple expression of the tunnel conductance of the SBD:

$$G=SD\exp(-2\kappa d), \tag{9}$$

where

$$D=\frac{2e^2}{h}\frac{m^*_{\mathrm{InAs}}}{2\pi\hbar^2}E_F. \tag{10}$$

Here E_F is the Fermi energy measured from the bottom of the conduction band of an InAs.

In Fig. 8, we plot the conductance-barrier thickness re-

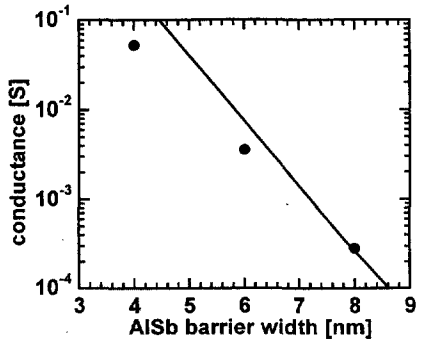

FIG. 8. Conductance-barrier width relation of AlSb–InAs SBD with a diameter of 100 μm. The dots (●) are experimental data. The solid curve is calculated from Eq. (9).

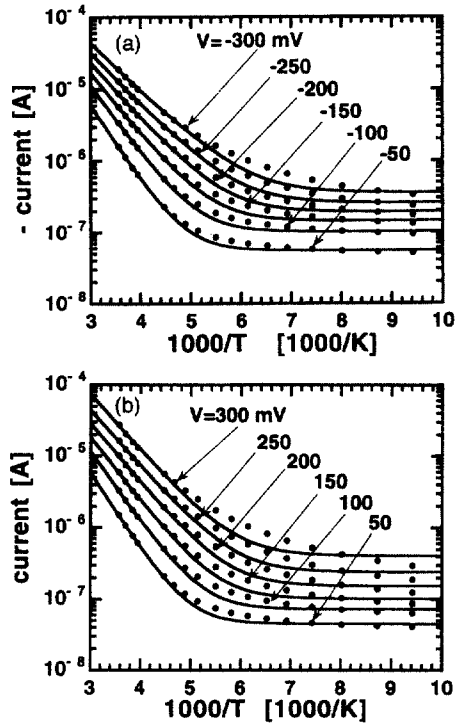

FIG. 9. Temperature dependence of the current through the AlSb–InAs SBD with a barrier thickness of 10 nm at different voltages (a) negatively biased and (b) positively biased. Dots (●) are experimental data and solid curves are the best fitted lines for the function (11).

lation. From the fitting of the experimental data, the parameter is estimated to be $\kappa=0.062\pi/a$. From the dopant concentration in an InAs contact layer, the Fermi energy in an InAs undope layer is estimated to be between 0.25 and 0.30 eV above the top of the AlSb valence band. As shown in Fig. 7, this experimentally obtained imaginary vector κ shows a good agreement with two-band model. Therefore, we conclude that the bulk current through the AlSb barrier is caused by the tunneling through the AlSb barrier influenced by the AlSb band structure.

For the parameter D, the difference between the experimental value 9.6×10^{8} S/m^2 and theoretical value 1.8×10^{11} S/m^2 is large. The value of conductance is quite sensitive to the change of κ due to its exponential dependence. We consider that if we employ a more elaborate model which includes multivalley band structure effect, the fit with the experimental data will be even better.

V. THE ORIGIN OF THE SURFACE CURRENT

As discussed in Sec. III, the thermally activated surface current dominates the current through the AlSb SBDs with a barrier thickness larger than ~8 nm. To clarify the mechanism of the conduction, we investigated the temperature dependence of the current through the AlSb SBD with a barrier thickness of 10 nm at different voltages (see Fig. 9). At low temperatures (<100 K), the current does not change with the temperature, since the tunneling current dominates the total current through the AlSb SBD. At high temperatures (>150 K), the current increases with the temperature due to the thermal activation of the current. Each current-temperature

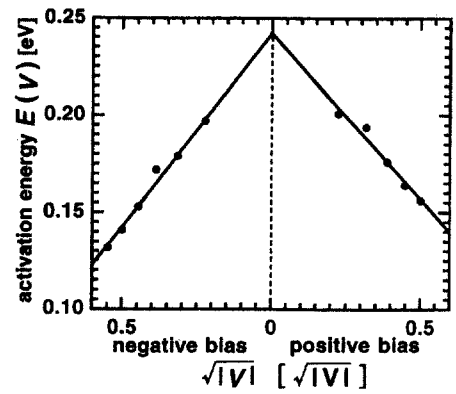

FIG. 10. Dots (●) is the activation energy versus applied voltage relation obtained from the fitting in Fig. 9. The solid line is the best fitted line for the function (12).

curve is well fitted with the simple two-component current model in which the total current I consists of a thermally activated current and a tunneling current in the following way:

$$I(V)=I_0(V)\exp[-E(V)/k_BT]+I_{\text{tunnel}}(V), \tag{11}$$

where V is the applied voltage, k_B is the Boltzmann's constant, and T is the temperature. In Fig. 10, we plot the activation energy $E(V)$ obtained from the fitting with respect to $\sqrt{|V|}$. We note that the activation energy is well fitted by the relation:

$$E(V)=E_{i0}-\alpha e\sqrt{|V|}, \tag{12}$$

where

$E_{i0}=0.24$ eV, $\alpha=0.17$ V$^{1/2}$ for positive bias voltage,
$E_{i0}=0.24$ eV, $\alpha=0.20$ V$^{1/2}$ for negative bias voltage (experimental).

There are two models which recognize such dependence of the activation energy on the applied voltage; one is the Poole–Frenkel emission model in which electrons are emitted thermally from the band-gap capture state in the barrier and the other is the Schottky emission model in which electrons are emitted thermally from the electrode to the barrier lowered by an image potential.[21] In the Poole–Frenkel model, the coefficient α is given by

$$\alpha=\sqrt{\frac{e}{\pi\epsilon d}}=0.203 \text{ V}^{1/2} \text{ (theoretical)}, \tag{13}$$

where ϵ is $14\epsilon_0$ (which is the permittivity of the AlSb), where ϵ_0 is the permittivity of vacuum. This value of α coincides well with the experimentally obtained value. On the other hand, in the Schottky emission model the coefficient is given by $\alpha=\sqrt{e/4\pi\epsilon d}=0.102$ V$^{1/2}$ and is different from the experimental value. Therefore we conclude that the origin of the surface current is the conduction through band-gap surface states at the AlSb surface based on the Poole–Frenkel emission mechanism with an ionization energy of 0.24 V. The oxidation or fabrication process damage such as etchant ion bombardment may induce such surface states.

The ionization energy of 0.24 V suggests that the band-gap surface levels at the AlSb surface lie 0.24 eV below the

top of the AlSb barrier. If the top of the AlSb barrier at the surface is equal to that in the bulk, the surface level is higher than the Fermi level in the emitter by about 1 eV. In this case, the surface level is too high for electrons to inject into the surface level within the range of voltages applied in the present experiment. Therefore, the AlSb barrier at the surface must be lower than that in the bulk. The breaking of the translational symmetry at the surface or the change of the material at the surface due to, for example, oxidation, may be responsible for the barrier height lowering.

VI. CONCLUSION

PVR for AlSb–InAs RTDs decreases with decreasing its diameter due to a thermally activated surface current. To clarify the origin of the surface current, we have investigated the $I(V)$ characteristics of the AlSb–InAs SBDs with various AlSb barrier thicknesses and various diode diameters from 2–100 μm at various temperatures.

For the AlSb–InAs SBD with barrier thickness less than about 8 nm, a current proportional to the area of the diode dominates over the whole current and is independent of temperatures. The dependence of the conductance on the AlSb barrier thickness is reasonably explained by the calculation of the tunnel probability based on the *sp* two-band model. Therefore we conclude unambiguously that the bulk current is attributed to the tunneling current through the AlSb barrier.

For the AlSb–InAs SBD with barrier thickness larger than about 8 nm, we observed a thermally excited current proportional to the surface current as we observed for the AlSb–InAs RTD. From the dependence of the current at various voltages on temperatures, we conclude that the surface current is caused by the conduction through band-gap surfaces states at the AlSb barrier based on the Poole–Frenkel mechanism with ionization energy of 0.24 eV.

ACKNOWLEDGMENTS

The authors would like to thank Dr. S. Usui and Dr. Y. Mori for encouragement. They are also grateful to T. Shimada for her technical assistance. This work was performed under the management of FED as a part of the MITI R&D program (Quantum Functional Devices Project) supported by NEDO.

[1] M. A. Reed, J. N. Randall, R. J. Aggarwal, R. J. Matyi, T. M. Moore, and A. E. Wetsel, Phys. Rev. Lett. **60**, 535 (1998).
[2] B. Su, V. J. Goldman, and J. E. Cunningham, Phys. Rev. B **46**, 7644 (1992).
[3] M. Tewordt *et al.*, Phys. Rev. B **49**, 8071 (1994).
[4] S. Tarucha, D. G. Austing, T. Honda, R. J. van der Hage, and L. P. Kouwenhoven, Phys. Rev. Lett. **77**, 3613 (1996).
[5] K. Nomoto, T. Suzuki, K. Taira, and I. Hase, Jpn. J. Appl. Phys., Part 2 **33**, L1142 (1994); Phys. Rev. B **55**, 2523 (1997).
[6] For a review, see *Physics of Quantum Electron Devices*, edited by F. Capasso (Springer, New York, 1990).
[7] L. F. Luo, R. Beresford, and W. I. Wang, Appl. Phys. Lett. **53**, 2320 (1988).
[8] J. R. Sördenström, E. R. Brown, C. D. Parker, L. J. Mahoney, J. Y. Yao, T. G. Andersson, and T. C. McGill, Appl. Phys. Lett. **58**, 275 (1991).
[9] T. E. Fischer, F. G. Allen, and G. W. Gobeli, Phys. Rev. **163**, 703 (1967).
[10] A. G. Milnes and A. Y. Polyakov, Mater. Sci. Eng., B **18**, 237 (1993).
[11] R. E. Carnahan *et al.*, Appl. Phys. Lett. **62**, 1385 (1993).
[12] K. Nomoto, K. Taira, T. Suzuki, I. Hase, H. Hiroshima, and M. Komuro, Appl. Phys. Lett. **70**, 2025 (1997).
[13] T. Schmidt, M. Tewordt, R. J. Haug, K. v. Kliting, B. Shönherr, P. Grambow, A. Förster, and H. Lüth, Appl. Phys. Lett. **68**, 838 (1996).
[14] M. Ozeki, K. Kodama, M. Takikawa, and A. Shibatomi, J. Vac. Sci. Technol. **21**, 438 (1982).
[15] J. H. Zhao, IEEE Trans. Electron Devices **37**, 1235 (1990).
[16] J. H. Zhao, R. Hwang, and Chang, IEEE Trans. Electron Devices **40**, 1172 (1993).
[17] V. R. Balakrishnan, Vikaram Kumar, and Subhasis Ghosh, IEEE Trans. Electron Devices **44**, 1060 (1997).
[18] T. Ando and S. Mori, Surf. Sci. **113**, 124 (1982).
[19] T. B. Boykin, Phys. Rev. B **51**, 4289 (1995).
[20] G. A. Sai-Halasz, L. Esaki, and W. A. Harrison, Phys. Rev. B **18**, 2812 (1978).
[21] S. M. Sze, *Physics of Semiconductor Devices* (Wiley, New York, 1981).